https://doi.org/10.5194/egusphere-2026-1917
Preprint. Discussion started: 20 May 2026

A Revised Framework for Classifying Organic Aerosols using Wavelength-dependent Absorption Properties

Susan Mathai [1,2,a], Gregory L Schuster (Ret.)[1], Michael A Shook [1], and Luke D Ziemba [1]

[1]NASA Langley Research Center, Hampton, USA
[2]Oak Ridge Associated Universities, Oak Ridge, USA
[a]Currently at University of Wyoming, Laramie, USA

Correspondence: Susan Mathai (smathai@uwyo.edu) and Luke D Ziemba (luke.ziemba@nasa.gov)

Abstract. The representation of organic aerosols (OA) in global climate models fails to account for the wide range of species found in the atmosphere. Previous studies have observed that the optical parameters of OA species vary depending on the source from which they are emitted, as well as on their physical and chemical characteristics. However, accounting for all OA species in climate models is not practical. Hence, we have grouped OA species according to their optical parameters and physico-chemical characteristics. We classified OA as strongly absorbing brown carbon (S-BrC), moderately absorbing brown carbon (M-BrC), weakly absorbing brown carbon (W-BrC) and very weakly absorbing brown carbon (VW-BrC). We defined thresholds based on the imaginary refractive index (IRI) for a broad wavelength range from 300 to 550 nm. The classification demonstrates clear optical separation at 350-500 nm, with mass absorption coefficient (MAC) values spanning two orders of magnitude from VW-BrC (0.004 m^2/g) to S-BrC (1 m^2/g) at 400 nm. Representative species from each category were suggested as surrogates. This choice of species includes both absorbing and scattering OA and enables more accurate representation of OA in climate models and satellite retrievals, improving aerosol radiative forcing estimates.

1 Introduction

Carbonaceous aerosols are carbon-containing compounds with the presence of hydrogen and oxygen. These aerosols are broadly classified into two main categories: black carbon (BC) and organic aerosols (OA). BC compounds can be distinguished based on their unique physical properties such as: strong light absorption in the visible region, resistance to high temperature of about 4000K and insolublity in water as well as other organic solvents (Bond et al., 2013). OA are a collection of different species broadly classified into primary OA (POA) and secondary OA (SOA) with varying physical properties. POA are emitted as particles into the atmosphere directly from the source and, SOA are formed through gas phase oxidation of volatile organic compounds (VOC) such as α-pinene, toluene, etc. (Liu et al., 2015, 2013b; Kanakidou et al., 2005). The SOA and POA contain a variety of molecular aggregates and chromophores such as humic-like substances (HULIS) formed by cloud processing and oligomerization (Graber and Rudich, 2006; Andreae and Gelencsér, 2006). These HULIS comprise small organic molecules

https://doi.org/10.5194/egusphere-2026-1917
Preprint. Discussion started: 20 May 2026

such as nitrocatechols, aromatic carboxylic acids, etc. (Laskin et al., 2015; Claeys et al., 2012; Graber and Rudich, 2006). The molecular complexity of OA arises due to the variety of emission sources such as forest fires, biomass burning, residential heating, and biogenic release (Ramanathan et al., 2007; Chakrabarty et al., 2010) as well as the atmospheric processing of OA (Powelson et al., 2014; De Haan et al., 2009; Nguyen et al., 2012; Laskin et al., 2015). The wavelength dependence of OA absorption and scattering is similarly heterogeneous, governed by physical and chemical characteristics that cannot be captured by representing them as single entity. Hence, variability in composition and atmospheric processing leads to different optical properties.

The molecular complexity of OA can be expressed through a set of optical parameters such as refractive index (RI), mass absorption coefficient (MAC), absorption Ångström exponent (AAE), and single scattering albedo (SSA). In situ and laboratory observations consistently show that OA span a continuum of RI and AAE that depend on emission source, chemical composition, mixing state, and atmospheric aging (Saleh, 2020; Saleh et al., 2014; Sumlin et al., 2018). For instance, tarballs (TBs), a highly viscous and spherical absorbing OA, have a huge uncertainty associated with its absorption. The highest reported value (0.28 at 532 nm) for the Imaginary Refractive Index (IRI) of TB is 2 orders of magnitude higher than the lowest reported IRI value (0.002 at 532nm) (Mathai et al., 2023; Alexander et al., 2008; Chakrabarty et al., 2010). Furthermore, studies observed that SOA produced from VOCs such as α-pinene through high NO_x photo-oxidation and ozonolysis had negligible absorption with an IRI less than 0.003 in the UV-visible region (Nakayama et al., 2010, 2012). However, some SOAs formed from toluene through high NO_x photo-oxidation showed an order of magnitude higher IRI (0.015 at 405 nm) than SOA formed from α-Pinene (Zhong and Jang, 2011; Liu et al., 2015). A more detailed classification of OA based on light absorption will lead to a more accurate implementation into climate models.

Previous studies have explored various approaches to classifying OA based on their optical and physicochemical properties (Saleh, 2020; Liu et al., 2015; Sumlin et al., 2017). Liu et al. (2015) and Sumlin et al. (2017) developed classification schemes by establishing IRI thresholds for absorbing OA. Their classifications encompassed anthropogenic OA derived from toluene and xylene, biogenic OA from α-pinene and limonene, and various brown carbon (BrC) types including fulvic acid, tar balls, HULIS, and urban BrC. Furthermore, Saleh (2020) proposed a four-category classification system for OA based on absorption properties at 550 nm, which incorporated additional physicochemical parameters such as solubility, volatility, and molecular size. Despite these advances, a comprehensive classification framework that simultaneously accounts for wavelength-dependent absorption, emission sources, and volatility characteristics remains lacking. This gap highlights the need for a more integrated approach to OA classification that can better capture the full complexity of atmospheric organic aerosols.

Despite the weight of evidence, many global models still reduce OA to a single, often non-absorbing (Alvarado et al., 2016), RI as described in the OPAC database (Hess et al., 1998), a simplification that propagates systematic biases in aerosol radiative effects and, ultimately, in estimates of radiative forcing. Bridging the gap between observational data and model representation demands a careful, measurement-informed classification of OA optical properties, enabling realistic, wavelength-dependent inputs that can be integrated into global models. Such a framework is essential for reducing uncertainty in aerosol-radiation interactions and for improving confidence in climate projections. Hence, the above mentioned inconsistencies suggest that there needs to be a new database with updated optical parameters from recent literature that can be adapted into climate models

https://doi.org/10.5194/egusphere-2026-1917
Preprint. Discussion started: 20 May 2026

for more accurate results. This study aims to provide clear thresholds accounting for the large variability in OA species so that it can be represented more accurately in climate calculations.

The classification scheme for OA developed in this study will be integrated into the Table of Aerosol Optics (TAO), a new database currently in development. TAO is designed to provide the scientific community with access to spectrally resolved optical properties of the major aerosol types, including BC, OA, dust, and others, accounting for their shape and hygroscopicity. This platform will serve researchers across multiple disciplines, from climate modelers requiring aerosol optical parameters for radiative transfer calculations to remote sensing scientists interpreting satellite retrievals and field campaign researchers analyzing in situ measurements.

2 Methodology

For this analysis, we compiled literature values for size distribution, density, and RI for each OA species (Table 1). We refer to OA as total particulate organic matter suspended in the atmosphere. It is important to understand the difference between OA, and organic carbon (OC). OC represents only the mass of carbon atoms in organic compounds, while OA includes the total mass of organic compound encompassing carbon and all associated elements (H, O, N, S etc.). These parameters served as inputs to generate the optical parameters (i.e., MAC and SSA).

2.1 Computational methods used to generate optical properties of organic aerosols

In this study, the optical parameters of OA, such as MAC, SSA, and other metrics were calculated by applying Mie theory using the Wiscombe code (Wiscombe, 1980). To represent the aerosol particle size distribution, a normalized lognormal number size distribution was employed, as expressed by the following equation:

$$\frac{dN}{d\ln r} = \frac{N_0}{\sqrt{2\pi}\ln\sigma_g}\exp\left(\frac{-(\ln r - \ln r_{mdn,N})^2}{2\ln^2\sigma_g}\right) \quad (\mathrm{cm}^{-3}) \tag{1}$$

where r represents the particle geometric radius, r_{mdn} is the number median radius, and σ_g is the geometric standard deviation. These values — r, r_{mdn}, and σ_g — were obtained or adopted from field campaigns reported in the literature (Table 1). The total number concentration of particles, N_0, is normalized such that:

$$N_0 = \int \frac{dN}{d\ln r} d\ln r = 1\,\mathrm{cm}^{-3}. \tag{2}$$

Each size distribution represents region-specific attributes (e.g., season, location) or source-specific conditions (e.g., fuel type, combustion process) characteristic of the OA species. In addition to the size distribution, the RI and particle density reported for individual aerosol species were utilized as input for computing the optical parameters. The *absorption coefficient*, ξ_{abs}, was calculated using the absorption cross section for a particle, C_{abs}, which is defined as:

$$C_{abs} = Q_{abs} G_p(r), \tag{3}$$

where Q_{abs} is the dimensionless absorption efficiency calculated using Mie theory, and $G_p(r) = \pi r^2$ is the geometric cross-sectional area of a spherical particle.

https://doi.org/10.5194/egusphere-2026-1917
Preprint. Discussion started: 20 May 2026

Table 1. Lognormal parameters (Geometric standard deviation (σ_g) and median radius (r_{mdn})) of the size distribution, density (ρ), and RI reference of each OA species used as inputs to generate the optical parameters.

OA Species	Size distribution			Density		RI
	σ	r_{mdn}	Reference	ρ	Reference	Reference
Fresh TBs 1	1.6	0.112	Adachi et al. (2019)	1.5	Sedlacek III et al. (2018)	Alexander et al. (2008)
Fresh TBs 2	1.6	0.112	Adachi et al. (2019)	1.5	Sedlacek III et al. (2018)	Chakrabarty et al. (2023)
Aged TBs	1.6	0.112	Adachi et al. (2019)	1.5	Sedlacek III et al. (2018)	Mathai et al. (2023)
wiBrC	1.53	0.095	Rissler et al. (2006)	1.2	Cheng et al. (2019)	Hoffer et al. (2006); Kirchstetter et al. (2004)
Lab TBs	1.6	0.112	Adachi et al. (2019)	1.5	Sedlacek III et al. (2018)	Li et al. (2019)
Toluene with NO_x	1.79	0.068	Hussein et al. (2004)	1.2	Cheng et al. (2019)	Liu et al. (2015)
wsBrC	1.53	0.095	Rissler et al. (2006)	1.2	Cheng et al. (2019)	Washenfelder et al. (2013)
m-Xylene with NO_x	1.79	0.068	Hussein et al. (2004)	1.2	Cheng et al. (2019)	Liu et al. (2015)
Toluene SOA	1.79	0.068	Hussein et al. (2004)	1.2	Cheng et al. (2019)	Liu et al. (2015)
m-Xylene SOA	1.79	0.068	Hussein et al. (2004)	1.2	Cheng et al. (2019)	Liu et al. (2015)
Catechol	1.53	0.095	Rissler et al. (2006)	1.2	Cheng et al. (2019)	Liu et al. (2013b)
Alpha-Pinene	1.53	0.095	Rissler et al. (2006)	1.2	Cheng et al. (2019)	Liu et al. (2013b)
Limonene	1.53	0.095	Rissler et al. (2006)	1.2	Cheng et al. (2019)	Liu et al. (2013b)
OPAC-Insoluble	2.51	0.47	Hess et al. (1998)	2	Hess et al. (1998)	Hess et al. (1998)
OPAC-Water-soluble	2.24	0.021	Hess et al. (1998)	1.8	Hess et al. (1998)	Hess et al. (1998)

Accordingly, the absorption coefficient can be formulated as:

$$\xi_{abs} = \int Q_{abs}(m,r,\lambda) G_p(r) \frac{dN}{d\ln r} d\ln r \qquad (\mathrm{Mm}^{-1}), \tag{4}$$

where λ is the wavelength of incident light, and m is the complex refractive index. Note that ξ_{abs} is expressed in inverse megameters (Mm^{-1}). The MAC, or specific absorption, was determined as the ratio of the absorption coefficient to the dry aerosol mass:

$$\beta_{abs} \equiv \frac{\xi_{abs}}{M_d} \qquad (\mathrm{m}^2\mathrm{g}^{-1}), \tag{5}$$

where the dry aerosol mass per unit volume of air is represented as

$$M_d = \rho_d V_d = \rho_d \int V_p(r) \frac{dN_d}{d\ln r} d\ln r \qquad (\mu\mathrm{gm}^{-3}). \tag{6}$$

Here, ρ_d refers to the aerosol's dry density, and $V_p(r)$ is the particle volume, expressed as $V_p(r) = \frac{4}{3}\pi r^3$ for spherical particles.

https://doi.org/10.5194/egusphere-2026-1917
Preprint. Discussion started: 20 May 2026

3 Results

3.1 Classification of Organic Aerosols

We classify OA into two primary categories: (1) BrC and (2) scattering OA (Scat OA). The BrC category is further subdivided into four distinct types: water-insoluble brown carbon (wiBrC), water-soluble brown carbon (wsBrC), fresh tarballs (Fresh TBs), and aged tarballs (Aged TBs). While tarballs are technically a subset of water-insoluble BrC, we treat them as separate categories due to their unique identification in the literature as a specific BrC morphology with distinctly different reported RI values. Furthermore, Scat OA are subclassified into: anthropogenic OA (Anthro OA) and biogenic OA (Bio OA). Anthro OA are formed from aromatic VOCs such as Toluene, Xylene, etc. emitted from anthropogenic sources, while Bio OAs are formed from VOCs such as $alpha$-pinene, limonene etc.

Table 2 compares the classification of OA in this study with those presented in previous studies (Hess et al., 1998; Saleh et al., 2014; Saleh, 2020). Early aerosol optical databases such as OPAC (Hess et al., 1998) represented OA using two categories based on solubility. Water-insoluble organics consist mostly of soil particles with organic material, while water-soluble organics originate from gas-to-particle conversion and include sulfates, nitrates, and other organic substances. Both OPAC categories were characterized as weakly absorbing, without accounting for the diversity in OA absorption characteristics. More recently, Saleh et al. (2014) categorized OA as mixtures composed of low volatile organic carbon (LVOC), semi volatile organic carbon (SVOC), and extremely low volatile organic carbon (ELVOC). Their study further explains that ELVOCs are byproducts of OA formed after heating at high temperatures, which volatilizes LVOCs and SVOCs (the scattering components of OA). This process produces ELVOCs that are highly absorbing aerosols with an IRI greater than 0.1 at 400 nm, an order of magnitude higher than total OA (Saleh et al., 2014). Subsequently, (Saleh, 2020) classified OA into four categories based on their IRI at 550 nm: very weakly absorptive (VW-BrC), weakly absorptive (W-BrC), moderately absorptive (M-BrC), and strongly absorptive (S-BrC). Their S-BrC corresponds to ELVOC and exhibits IRI values greater than 0.1 at 550 nm.

Our classification scheme was developed by synthesizing optical property data from 12 studies reporting RI values for 13 different OA species across the shortwave spectral region (300 to 550 nm) (Figure 1). Following a similar approach to (Saleh, 2020), we classified the OA into four groups based on absorption strength: VW-BrC, W-BrC, M-BrC, and S-BrC. S-BrC corresponds to ELVOCs such as TBs and wi-BrC. M-BrC represents mixtures of LVOCs, SVOCs, and ELVOCs with a higher percentage of absorbing SVOC components, similar to water-soluble BrC. W-BrC and VW-BrC are mixtures of LVOCs, SVOCs, and ELVOCs with higher percentages of SVOC and LVOC components, similar to anthro SOA and bio SOA.

https://doi.org/10.5194/egusphere-2026-1917
Preprint. Discussion started: 20 May 2026

Table 2. Comparison of OC classification in this study to previous literature.

OC Family and Genus	Volatility (Saleh et al., 2014)	Absorption (Saleh, 2020)	OPAC (Hess et al., 1998)
ScatOA:			
Bio SOA	LVOC + SVOC + ELVOC	VW-BrC (Very weakly absorptive BrC)	Water-soluble organics
Anthro SOA	LVOC + SVOC + ELVOC	W-BrC (Weakly absorptive BrC)	Insoluble organics
BrC:			
wsBrC	LVOC + SVOC + ELVOC	M-BrC (Moderately absorptive BrC)	
wiBrC	ELVOC	S-BrC (Strongly absorptive BrC)	
Fresh TB	ELVOC	S-BrC (Strongly absorptive BrC)	
Aged TB	ELVOC	S-BrC (Strongly absorptive BrC)	

3.2 Classification at different wavelengths

We have developed a classification scheme based on IRI values that accounts for the wavelength-dependent nature of light absorption by OA species to systematically organize the optical properties of absorbing and scattering OA (Figure 1). This categorization reflects both the magnitude of absorption and the volatility characteristics. Importantly, the boundaries between these categories are wavelength-dependent. This wavelength dependence is particularly pronounced in the ultraviolet to visible range (300-550 nm), where BrC absorption peaks and then decreases toward longer wavelengths. In the following subsections, we detail the IRI threshold criteria for each category and provide the scientific rationale for classifying specific aerosol types based on their formation mechanisms, chemical properties, and measurement techniques. Horizontal lines representing the IRI for BC and for AERONET (Aerosol Robotic Network) detection limits are also shown in Figure 1 for context. AERONET observations provide column retrievals of IRI, but is only sensitive to W-BrC and VW-BrC at shorter wavelengths.

3.2.1 Strongly Absorbing Brown Carbon (S-BrC)

We used literature data from tarballs analyzed using EELS (Mathai et al., 2023; Alexander et al., 2008; Chakrabarty et al., 2023) and acetone-extracted OA (Kirchstetter et al., 2004) to establish the classification threshold for S-BrC. S-BrC represents the most highly absorbing OA in our classification scheme, defined by IRI values greater than 0.03 at 550 nm (Figure 1, Table 3). This category primarily consists of ELVOC that can persist in the atmosphere for extended periods. For instance, tarballs analyzed using electron energy loss spectroscopy (EELS) and acetone-extracted OA are atmospheric aerosols with a volatile component partly or completely lost during the measurement technique. Literature values for tarball IRI using EELS technique at 550 nm ranged from 0.0325 to 0.274 for samples collected from ambient sources. It is important to note that the LVOCs and SVOCs are removed during interactions with intense electron beams (Saleh, 2020). In addition, LVOCs and SVOCs are also removed during the solvent extraction of organic aerosols, leading us to classify them as wiBrC.

https://doi.org/10.5194/egusphere-2026-1917
Preprint. Discussion started: 20 May 2026

3.2.2 Moderately Absorbing Brown Carbon (M-BrC)

The M-BrC category includes species with IRI values ranging from 0.0003 to 0.03 at 550 nm (Figure 1, Table 3). An IRI of 0.0003 at 550 nm is essentially non-absorbing, but we classify these aerosols as moderately absorbing because they have significant absorption at the blue and UV wavelengths. While both S-BrC and M-BrC are formed during high-temperature combustion, M-BrC includes species having mixtures of ELVOC, SVOC, and LVOC. In this study, M-BrC contains three species: Laboratory tarballs (Li et al., 2019), Savanna River Fulvic Acid (SRFA; Washenfelder et al., 2013), and Toluene-derived SOA with NO_x (Liu et al., 2015).

1. Laboratory tarballs: These tarballs were produced under controlled laboratory conditions and phase-separated into water soluble and insoluble components. Laboratory tarballs exhibit a known amount of water-soluble and water-insoluble components of BrC resulting in moderate absorption. Unlike tarballs that have been impacted by EELS technique, in (Li et al., 2019), optical properties were measured using the cavity enhanced technique which minimizes the evaporation of SVOCs and LVOCs.

2. Savanna River Fulvic Acid (SRFA): SRFA is often used as a surrogate for humic-like substances in aged aerosol and exhibits moderately absorbing characteristics. A study by (Washenfelder et al., 2013) used a cavity enhanced technique to derive the RI of SRFA for a wavelength range of 360 to 420 nm by aerosolizing the pure compound using distilled water, ensuring accurate optical property determination. The IRI for a wavelength range of 420 to 550 nm was obtained from the IRI values of SRFA reported by Liu et al. (2015) using UV-visible spectroscopy technique. The moderately absorbing nature of SRFA, combined with its representation of aged atmospheric organic matter, appropriately places it within the M-BrC category.

3. Toluene-derived SOA with NO_x: Toluene with OH, Toluene-derived with NO_x, Xylene with OH, and Xylene-derived with NO_x represent secondary organic aerosols from aromatic precursors that are generally less absorbing than primary combustion products (Laskin et al., 2015). However, multiple studies have documented that Toluene-derived SOA with NO_x demonstrates appreciable absorption coefficients at near-UV wavelengths (Liu et al., 2015; Zhong and Jang, 2011; Nakayama et al., 2013). This enhanced absorption, attributed to NO_x-facilitated chromophore formation during the oxidation process, elevates Toluene-derived SOA with NO_x from the weakly absorbing category to the M-BrC classification. The NO_x-enhanced formation pathway produces nitrogen-containing compounds that contribute to moderate absorption properties at 550 nm, distinguishing it from other aromatic SOA species.

3.2.3 Weakly Absorbing Brown Carbon (W-BrC)

Secondary BrC emissions from aromatic VOCs typically exhibit weaker absorption than BrC emissions from smoldering combustion and BC-producing combustion processes (Saleh, 2020; Saleh et al., 2014). Consequently, the W-BrC and VW-BrC categories consist of SOAs produced from aromatic VOCs. At 500 and 550 nm wavelengths, our classification includes all the species in W-BrC and VW-BrC category, which encompasses SOAs derived from Toluene, Xylene, Xylene with NO_x,

https://doi.org/10.5194/egusphere-2026-1917
Preprint. Discussion started: 20 May 2026

α-Pinene, Limonene, and Catechol. The W-BrC classification corresponds to aerosols with IRI values ranging from 0.0001 to 0.0006 at 500 nm and 0.0001 to 0.0003 at 550 nm.

3.2.4 Very Weakly Absorbing Brown Carbon (VW-BrC)

At shorter wavelengths ranging from 300 to 450 nm, we can distinguish between two categories based on precursor source: W-BrC containing SOAs from anthropogenic VOCs and VW-BrC containing SOAs from biogenic VOCs. The W-BrC category consists of SOAs produced by photooxidation of Toluene and m-Xylene in both the presence and absence of NO_x, as well as Catechol. The IRI values for SOAs from Toluene and m-Xylene are based on (Liu et al., 2015), who used spectroscopic ellipsometry to determine the complex refractive index. The VW-BrC category comprises SOAs from biogenic VOCs such as α-Pinene and Limonene. The IRI values for SOAs from biogenic VOCs were determined using spectroscopic ellipsometry in a previous study by (Liu et al., 2013b).

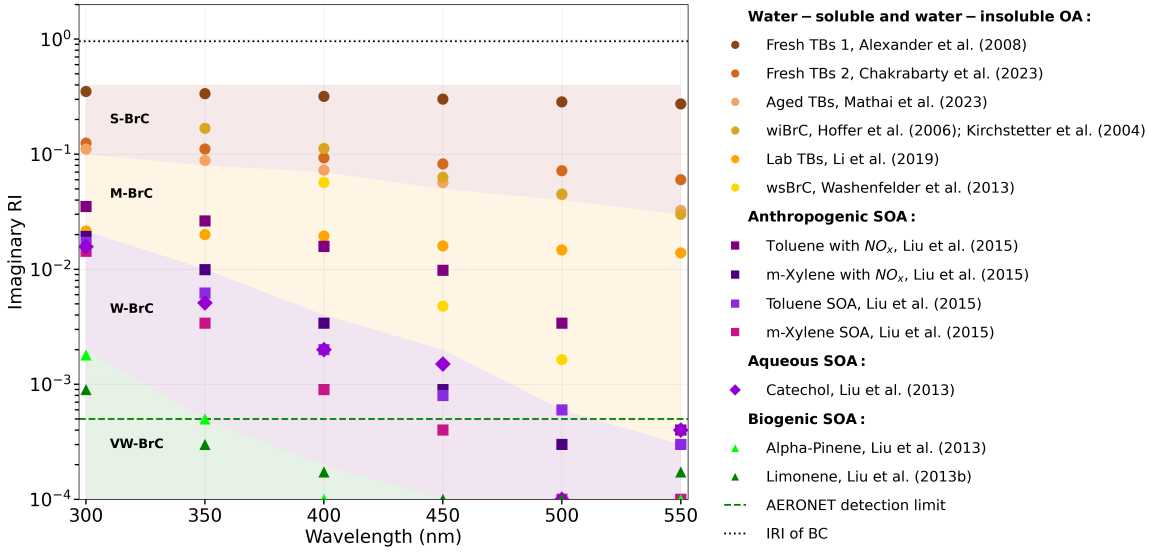

Figure 1. Organic aerosols from different sources are classified into four groups based on their Imaginary RI reported by previous studies as very weakly absorbing (VW-BrC, green), weakly absorbing (W-BrC, purple), moderately absorbing (M-BrC, light brown), and strongly absorbing (S-BrC, dark brown). The green dashed line shows the detection limit of AERONET (Dubovik and King, 2000) and the black dotted line marks the IRI of BC (Moteki et al., 2023).

https://doi.org/10.5194/egusphere-2026-1917
Preprint. Discussion started: 20 May 2026

Table 3. Threshold IRI values at different wavelengths for the four BrC groups.

Wavelength (nm)	VW-BrC	W-BrC	M-BrC	S-BrC
300	< 0.002	0.002 - 0.0215	0.0215 - 0.1	0.1 - 0.4
350	< 0.0005	0.0005 - 0.01	0.01 - 0.08	0.08 - 0.4
400	< 0.0002	0.0002 - 0.004	0.004 - 0.07	0.07 - 0.4
450	< 0.0001	0.0001 - 0.002	0.002 - 0.05	0.05 - 0.4
500	< 0.0001	0.0001 - 0.0006	0.0006 - 0.04	0.04 - 0.4
550	< 0.0001	0.0001 - 0.0003	0.0003 - 0.03	0.03 - 0.4

3.3 Classification of OA based on MAC and SSA values

While, Sect.3.2 established classification criteria based on IRI values, we translate these thresholds into MAC space to provide an alternative metric for representing BrC aerosols. The MAC thresholds presented here correspond to the IRI-based boundaries defined earlier, offering a complementary framework. MAC values, expressed in units of m^2/g and explicitly calculated using the inputs from Table 1, offer a mass-normalized measure of aerosol light absorption that is particularly valuable for atmospheric modeling applications and direct comparisons with field measurements where aerosol mass concentrations are readily available. In this section, we present IRI based threshold in MAC space for the same four absorption categories (S-BrC, M-BrC, W-BrC, and VW-BrC) (Figure 2, Table 4). This dual classification approach allows researchers to utilize the metric most appropriate for their specific application. MAC boundaries generally show similar separation and wavelength-dependence as IRI values. However, a significant difference arises at 300 nm, where the IRI-based classification identifies four distinct categories, while the MAC values separating these categories are very closely spaced. Specifically, at 300 nm, OA that are clearly differentiated by IRI as S-BrC, M-BrC, and W-BrC in the wavelength range of 350-500 nm have MAC values that converge, resulting in classification boundaries with minimal separation. This narrow spacing between thresholds at 300 nm indicates that MAC-based classification has limited discriminating power at this wavelength, making it less robust for distinguishing among different BrC types and more susceptible to measurement uncertainties.

As shown in Figure 2, S-BrC, M-BrC, and W-BrC are distinctly separated at 550 nm, consistent with the classifications derived from the IRI-based approach (Figure 1). The MAC threshold for S-BrC at 550 nm is above 0.6 m^2/g (Table 4), aligning with previously reported results in the literature. For example, in a study by Hoffer et al. (2016), the MAC values of tarballs generated under varying sources and temperatures were reported to range from 0.8 to 2.5 m^2/g, which corresponds to the S-BrC category. It was further noted in the study that these tarballs were resistant to high electron beam making them relevant to be categorized as S-BrC. Another study by (Updyke et al., 2012) reports a MAC value of 0.9 m^2/g at 500 nm for acetone extracts from biomass burning aerosols from (Kirchstetter et al., 2004) which is consistent with the S-BrC threshold.

For the M-BrC category, MAC values at 550 nm are in the range of 0.01 to 0.64 m^2/g (Table 4). A study by Sedlacek III et al. (2018) computed the MAC values of laboratory-generated tarballs using the refractive index reported by Chakrabarty

https://doi.org/10.5194/egusphere-2026-1917
Preprint. Discussion started: 20 May 2026

et al. (2010). These MAC values, derived after burning wood samples in the laboratory and directly analyzing the particles without chemical extraction or electron beam interactions, were reported as 0.22 m^2/g. This falls within the defined M-BrC threshold, further supporting the reasoning that BrC particles analyzed without chemical treatments comprise a complex mixture of low-volatility organic compounds (LVOC), semi-volatile organic compounds (SVOC), and extremely low-volatility organic compounds (ELVOC). Another study by Dinar et al. (2008) reported the IRI of water soluble humic-like substances (HULIS) collected at various sites across Europe. The reported IRI at 532 nm was subsequently used by Updyke et al. (2012) to calculate the MAC, which was found to range from 0.07 to 1 m^2/g which is consistent with the M-BrC category in this study.

For W-BrC, a clear distinction from VW-BrC is only evident for wavelength ranging from 350 to 450 nm (Figure 2). Above 500 nm, the VW-BrC and W-BrC MAC values are indistinguishable. The reason for this grouping is evident in a study by (Romonosky et al., 2016), where the MAC values for biogenic SOA extrapolates to zero above 450 nm. The MAC value ranges for the W-BrC at 500 nm and 550 nm are 0.003 - 0.07 and 0.003 - 0.01 respectively. At 450 nm, the MAC values range from 0.016 to 0.22, which is again consistent with values reports by Romonosky et al. (2016) for Toluene and Xylene derived SOAs. To place these findings in the context of established aerosol optical databases, we compare our MAC values with those from the OPAC database (Figure 2), which provides widely-used parameterizations for aerosol modeling applications. The OPAC MAC value for water-soluble organic at 450 nm is 0.12 m^2/g, and for water-insoluble organic is 0.064 m^2/g which overlaps with our observed W-BrC range of 0.016 - 0.22 m^2/g. Our analysis suggests that absorption by water-soluble and water-insoluble OA (i.e., S-BrC and M-BrC) is systematically underestimated by OPAC, while biogenic SOA (VW-BrC) absorption has been overestimated. Additionally, OPAC fails to reproduce the significant wavelength dependence of MAC values.

For VW-BrC, the IRI demonstrates a sharper decline with increasing wavelength compared to other BrC types. This wavelength-dependent behavior limits the threshold definition for VW-BrC to wavelengths up to 450 nm. Based on the MAC values calculated in this study, the threshold for VW-BrC at 300 nm is defined as MAC ranging from 0.06 - 0.8 m^2/g (Table 4). This finding is consistent with the MAC value of about 0.07 m^2/g at 300 nm reported by Romonosky et al. (2016) for α-Pinene SOA. Additionally, Romonosky et al. (2016) provided MAC values for other biogenic SOAs, including isoprene, β-Pinene, Myrcene, and Limonene. These biogenic SOAs all exhibit MAC values below 0.1 m^2/g at 300 nm, supporting their inclusion in the VW-BrC category. The small MAC values observed in this study reinforces the placement of biogenic SOAs into the VW-BrC classification and highlights their small contribution to light absorption.

https://doi.org/10.5194/egusphere-2026-1917
Preprint. Discussion started: 20 May 2026

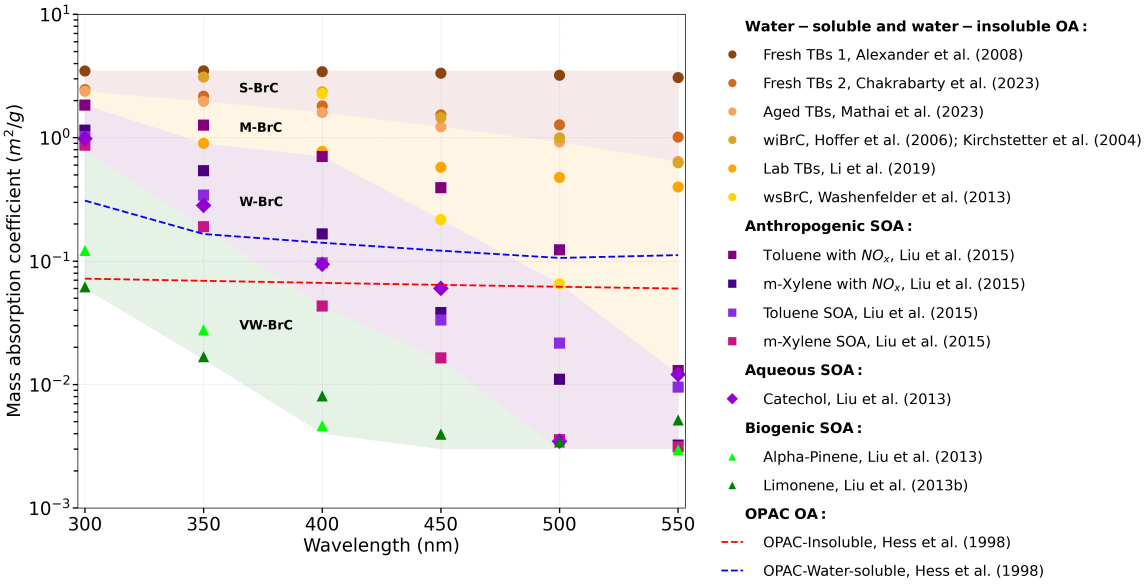

Figure 2. Thresholds for organic aerosol classes: very weakly absorbing (VW-BrC, green), weakly absorbing (W-BrC, purple), moderately absorbing (M-BrC, light brown), and strongly absorbing (S-BrC, dark brown) based on their MAC values calculated from the RI reported by previous studies in Figure 1. Based on the MAC values, characterization of the diversity of the species is better for wavelengths ranging from 350 nm to 450 nm. The red dashed line represent water-insoluble aerosol in OPAC model that consists mostly of soil particles with some amount of organic material and the blue dashed line represent the water-soluble aerosol in OPAC model that consists of various kinds of sulfates, nitrates, and organic water-soluble substances.

Table 4. Threshold MAC values (m^2/g) at different wavelengths for the four BrC groups.

Wavelength (nm)	VW-BrC	W-BrC	M-BrC	S-BrC
300	0.06 - 0.8	0.8 - 1.84	1.84 - 2.38	2.38 - 3.5
350	0.016 - 0.19	0.19 - 0.9	0.9 - 1.97	1.97 - 3.5
400	0.004 - 0.043	0.043 - 0.71	0.71 - 1.60	1.60 - 3.5
450	0.003 - 0.016	0.016 - 0.22	0.22 - 1.23	1.23 - 3.5
500	Combined with W-BrC	0.003 - 0.07	0.07 - 0.92	0.92 - 3.5
550	Combined with W-BrC	0.003 - 0.01	0.01 - 0.64	0.64 - 3.5

Complementing the MAC-based findings, SSA values provide another metric often used to describe aerosol absorption and are critical for radiative forcing calculations, as shown in Figure 3. Here, we see that SSA measurements can only discern two groups of OA at the 500 and 550 nm wavelengths because W-BrC and VW-BrC are dominated by scattering at those wavelengths (i.e., SSA $\simeq$ 1). Thus, SSA at 550 nm is useful for discriminating the tarballs and wiBrC of S-BrC from the M-

https://doi.org/10.5194/egusphere-2026-1917
Preprint. Discussion started: 20 May 2026

BrC. Across intermediate wavelengths (400 nm and 450 nm), SSA can discern three categories: S-BrC, M-BrC, and W-BrC. However, all four categoiries of OAs can be distinguished at the 300 nm wavelength (S-BrC, M-BrC, W-BrC and VW-BrC). Note that OPAC values for water-insoluble OA are only relevant for our S-BrC category and would underestimate SSA for all other categories. OPAC water-soluble SSA values can represent VW-BrC and W-BrC categories adequately, but overestimate SSA for M-BrC aerosols at lower wavelengths.

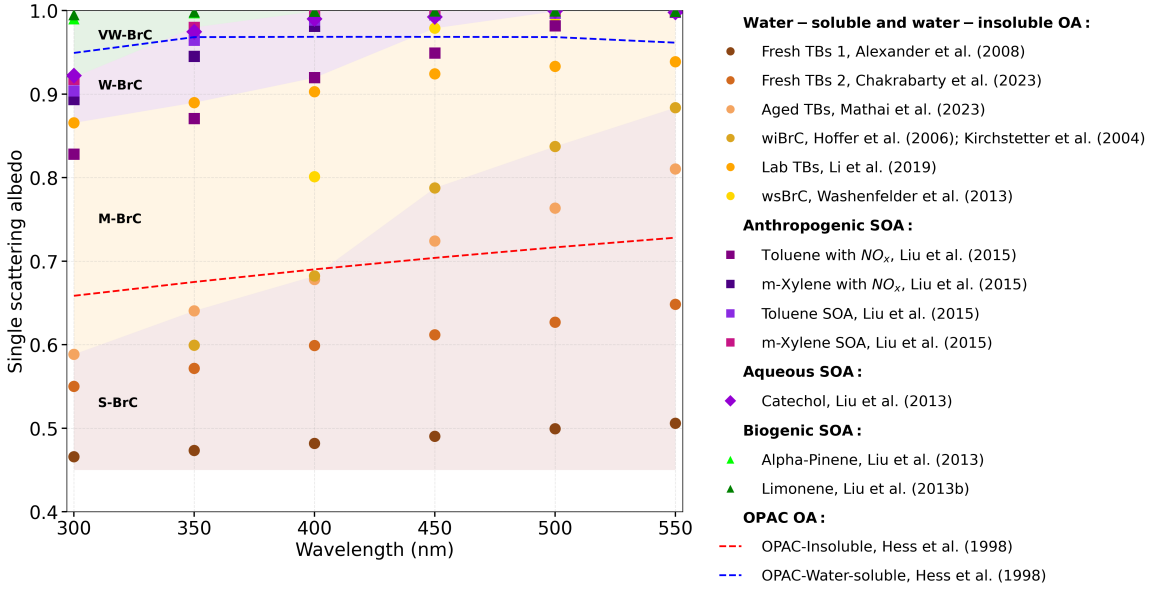

Figure 3. Thresholds for organic aerosol classes: very weakly absorbing (VW-BrC, green), weakly absorbing (W-BrC, purple), moderately absorbing (M-BrC, light brown), and strongly absorbing (S-BrC, dark brown) based on their SSA values calculated from the RI reported by previous studies in Figure 1. Based on the SSA values, characterization of the diversity of the species is best for shorter wavelength of 300 nm.Like for Figure 2, red and blue dashed lines represent water-insoluble and water-soluble values from OPAC for context.

Table 5. Threshold SSA values at different wavelengths for the four BrC groups.

Wavelength (nm)	VW-BrC	W-BrC	M-BrC	S-BrC
300	0.92 - 0.999	0.87 - 92	0.59 - 0.87	0.45 - 0.59
350	0.98 - 0.999	0.89 - 0.98	0.64 - 0.89	0.45 - 0.64
400	0.999	0.92 - 0.999	0.68 - 0.92	0.45 - 0.68
450	0.999	0.98 - 0.999	0.79 - 0.98	0.45 - 0.79
500	0.999	0.999	0.84 - 0.999	0.45 - 0.84
550	0.999	0.999	0.88 - 0.999	0.45 - 0.88

https://doi.org/10.5194/egusphere-2026-1917
Preprint. Discussion started: 20 May 2026

3.4 Suggested surrogate OA for each category

There are too many OA species in the atmosphere to simulate individually, so we carefully selected one species for each of our BrC categories to use as a surrogate based on data availability and relevance, as shown in Table 6. For example, several anthropogenic OAs exist in the atmosphere, including those derived from toluene, xylene, trimethylbenzene etc. (Olivier et al., 1996). However, incorporating each of these species into climate, weather, or air-quality models poses significant challenges. Among these, SOAs derived from Toluene and Xylene are the most abundant anthropogenic aromatics found in highly polluted urban areas (Odum et al., 1996; Ng et al., 2007). Additionally, Harley et al. (1992) identifies Toluene as a major aromatic compound, comprising 40% of aromatic emissions from mobile sources. Similarly, (Kleindienst et al., 2007) reports that 50% of aromatic SOA generated from a synthetic gasoline mixture in a smog chamber is Toluene-derived. Hence, we use Toluene derived SOA as the representative anthropogenic species.

Similarly, there are several types of Biogenic VOCs emitted from terrestrial vegetation including isoprene, monoterpenes, methanol, and sesquiterpenes, that collectively account for 90% of total non-methane VOC emissions (Guenther et al., 2006; Sindelarova et al., 2014; Wang et al., 2024). Although global isoprene emissions exceed those of monoterpenes, the SOA yield from monoterpenes is higher and leads to the formation of condensable products that contribute to SOA particle growth (Hoffmann et al., 1997; Arneth et al., 2008). Among monoterpenes, α-pinene (34%), β-pinene (17%), and trans-β-ocimene (23%) are the three major contributors to the global annual total over the 1980-2010 period (Sindelarova et al., 2014). Consequently, we use the RI of limonene to represent Biogenic SOA due to the availabiltiy of more spectrally resolved data, which overlaps with the RI of α-pinene as reported by (Liu et al., 2013b) (Table 6).

While some fractions of anthropogenic and biogenic OA can exhibit BrC properties under specific formation conditions (Laskin et al., 2015), the majority of conventional Anthropogenic and Biogenic OA demonstrates very low IRI (typically $< 10^{-2}$ at 370nm) (Liu et al., 2015, 2013b), making these components appropriately classified as scattering OA (Scat OA). BrC contains both water-soluble and insoluble components (Laskin et al., 2015). Often studies employ extraction techniques to study the optical properties of BrC using water or other polar solvents (like methanol, acetone etc.) (Wu et al., 2019; Liu et al., 2013a; Li et al., 2020; Kirillova et al., 2014). Hence, optical properties of water soluble and water insoluble components of BrC aerosols are studied separately (Kirillova et al., 2014). As a result, they can be subdivided based on their solubility, volatility, and viscosity into wsBrC, wiBrC, and Tarballs. Savanna River Fulvic Acid (SRFA) obtained from the International Humic Substances Society (IHSS) is often regarded as a reference model for comparing molecular size and hygroscopic growth of HULIS (Mo et al., 2017; Fan et al., 2012; Dinar et al., 2007). Hence, we used the RI of SRFA reported by (Washenfelder et al., 2013) and (Sumlin et al., 2017; Liu et al., 2015) to represent wsBrC species in the shortwave region. For wiBrC, we use the RI of three different species: acetone extracted OA (wiBrC), fresh tarballs, and aged tarballs (Table 6).

https://doi.org/10.5194/egusphere-2026-1917
Preprint. Discussion started: 20 May 2026

Table 6. RI, MAC, and SSA for the species selected to represent each class in TAO.

Class	Wavelength	Refractive Index	MAC	SSA
Fresh Tarballs	300	1.32 + 0.13i	1.44	0.54
	350	1.33 + 0.11i	1.38	0.56
	400	1.33 + 0.093i	1.26	0.6
	450	1.33 + 0.082i	1.15	0.63
	500	1.32 + 0.072i	1.02	0.66
	550	1.32 + 0.06i	0.87	0.7
Aged Tarballs	300	1.35 + 0.11i	1.42	0.55
	350	1.37 + 0.088i	1.32	0.6
	400	1.37 + 0.073i	1.18	0.65
	450	1.37 + 0.057i	0.99	0.71
	500	1.38 + 0.045i	0.82	0.76
	550	1.38 + 0.033i	0.62	0.82
wiBrC (Acetone extracted)	350	1.67 + 0.17i	4.65	0.6
	400	1.67 + 0.11i	3.53	0.68
	450	1.67 + 0.063i	2.18	0.79
	500	1.67 + 0.045i	1.50	0.84
	550	1.67 + 0.03i	0.94	0.88
wsBrC (SRFA)	400	1.68 + 0.057i	2.29	0.8
	450	1.65 + 0.0048i	0.22	0.98
	500	1.65 + 0.0016i	0.065	0.99
Anthropogenic OA (Toluene)	300	1.57 + 0.02i	1.02	0.90
	350	1.56 + 0.0062i	0.34	0.96
	400	1.55 + 0.002i	0.097	0.99
	450	1.54 + 0.0008i	0.033	0.99
	500	1.53 + 0.0006i	0.01	0.99
	550	1.53 + 0.0003i	0.009	0.99
Biogenic OA (Limonene)	300	1.55 + 0.0009i	0.062	0.99
	350	1.53 + 0.0003i	0.012	0.99
	400	1.52 + 0.0002i	0.008	0.99
	450	1.51 + 0.0001i	0.004	0.99
	500	1.51 + 0.0001i	0.003	0.99
	550	1.50 + 0.0002i	0.005	0.99

https://doi.org/10.5194/egusphere-2026-1917
Preprint. Discussion started: 20 May 2026

4 Conclusions

In this study, we have presented a comprehensive classification scheme for OA and demonstrated how this classification was adapted to select representative species for each category. OA were broadly classified into absorbing and scattering categories,which were further subdivided into four distinct categories based on the IRI and volatility properties of the species: VW-BrC, W-BrC, M-BrC, and S-BrC. The four categories exhibit distinct optical and physical characteristics spanning orders of magnitude in absorption.

VW-BrC, represented by biogenic OAs, displays extreme volatility and maximum scattering with MAC values <0.004 m^2/g at 450 nm. W-BrC, represented by anthropogenic OAs, is characterized by high volatility and scattering properties with MAC values ranging from 0.015-0.06 m^2/g at 450 nm. M-BrC, consisting of ws-BrC and mixtures of ws-BrC and wi-BrC, exhibits lower volatility and moderate absorbing properties with MAC values ranging from 0.2-0.55 m^2/g at 450 nm. Finally, S-BrC, composed of wi-BrC and tarballs, is characterized by the least volatility and strong absorption with MAC values >1 m^2/g, —a 100-fold increase over VW-BrC.

The classification boundaries are most prominent at shorter wavelengths (350-450 nm), where brown carbon absorption is strongest. At 450 nm, the upper bound IRI threshold for each successive category is approximately 10 times higher, providing clear optical separation between categories. Similarly, MAC-based thresholds are most distinct at 350, 400, and 450 nm, making these wavelengths optimal for OA classification. This wavelength dependence reflects the characteristic spectral absorption of brown carbon, which decreases toward longer wavelengths.

Our analysis demonstrates that, unlike OPAC where OA are represented by mostly-scattering species, atmospheric models must incorporate both absorbing and scattering OA to accurately capture their optical diversity. For instance, Kim et al. (2008) uses biogenic SOA to represent the OA in the climate model which again corresponds to only VW-BrC in our classification scheme. Furthermore, most climate models fail to account for the wavelength dependence of OA (Sand et al., 2021).The 100-fold difference in MAC values between S-BrC and VW-BrC underscores the critical importance of this expanded representation for radiative forcing calculations. Such variability also translates into large differences in aerosol absorption coefficients, which can modify the shortwave atmospheric heating rates by orders of magnitude in regions with significant OA loading. In addition, this variability poses a challenge for legacy satellite retrieval algorithms, which commonly assume non-absorbing or weakly absorbing aerosols. We recommend using a mixture of ws-BrC and wi-BrC for representing absorbing OA, and anthropogenic or biogenic secondary organic aerosols for scattering OA. This approach will enable climate modelers to better represent OA optical properties in radiative transfer calculations, potentially improving estimates of aerosol direct radiative forcing. The TAO classification scheme serves as a valuable resource for satellite retrieval algorithms and climate models requiring accurate aerosol optical properties.

4.1 Caveats and Limitations

The interpretation of VW-BrC and W-BrC categories at visible wavelengths is subject to detectability constraints. For instance, the IRI of VW-BrC above 400 nm, and W-BrC above 500 nm is below the detection limit of AERONET (Figure 1). However,

https://doi.org/10.5194/egusphere-2026-1917
Preprint. Discussion started: 20 May 2026

their IRI are above the detection limit of AERONET at shorter wavelengths. Hence, the absorption decreases substantially toward longer wavelengths, and in the visible range their IRI approach the detection limits of typical optical instruments.

In addition, computation of MAC and SSA values using Mie theory relies on several simplifying assumptions. These include the treatment of aerosols as homogeneous and spherical with externally mixed compositions and size distributions. Real atmospheric aerosols may deviate from these assumptions due to internal mixing, non-sphericity, and morphological complexity.

Code and data availability. The data and code supporting the findings of this study are available from the corresponding author upon reasonable request.

https://doi.org/10.5194/egusphere-2026-1917
Preprint. Discussion started: 20 May 2026

Author contributions. SM and GLS conceived the study and developed the model code. SM performed the calculations, analyzed the results and prepared the figures. SM wrote the manuscript with input from MAS, LDZ, and GLS. All authors reviewed and approved the final version.

Competing interests. The contact author has declared that none of the authors has any competing interests.

Acknowledgements. The authors thank Charles R. Trepte and the CALIPSO group for funding this project. We also thank the LARGE group for their support, guidance, and feedback. Susan Mathai's research was supported by the NASA Postdoctoral Program at NASA Langley Research Center, administered by Oak Ridge Associated Universities under contract with NASA. The authors used ChatGPT 4.1 to improve grammar, rephrase sentences for clarity, and assist in editing code for figure generation.

https://doi.org/10.5194/egusphere-2026-1917
Preprint. Discussion started: 20 May 2026

References

Adachi, K., III, A. S., Kleinman, L., Springston, S., Wang, J., Chand, D., Hubbe, J., Shilling, J., Onasch, T., Kinase, T., Sakata, K., Takahashi, Y., and Buseck, P.: Spherical tarball particles form through rapid chemical and physical changes of organic matter in biomass-burning smoke, Proc. Natl. Acad. Sci., 116, 18 689–18 694, https://doi.org/10.1073/pnas.1900129116, 2019.

Alexander, D., Crozier, P., and Anderson, J.: Brown Carbon Spheres in East Asian Outflow and Their Optical Properties, Science, 321, 833–836, 2008.

Alvarado, M. J., Lonsdale, C. R., Macintyre, H. L., Bian, H., Chin, M., Ridley, D. A., Heald, C. L., Thornhill, K. L., Anderson, B. E., Cubison, M. J., Jimenez, J. L., Kondo, Y., Sahu, L. K., Dibb, J. E., and Wang, C.: Evaluating model parameterizations of submicron aerosol scattering and absorption with in situ data from ARCTAS 2008, Atmospheric Chemistry and Physics, 16, 9435–9455, https://doi.org/10.5194/acp-16-9435-2016, 2016.

Andreae, M. O. and Gelencsér, A.: Black carbon or brown carbon? The nature of light-absorbing carbonaceous aerosols, Atmospheric Chemistry and Physics, 6, 3131–3148, 2006.

Arneth, A., Monson, R. K., Schurgers, G., Niinemets, U., and Palmer, P. I.: Why are estimates of global terrestrial isoprene emissions so similar (and why is this not so for monoterpenes)?, Atmospheric Chemistry and Physics, 8, 4605–4620, https://doi.org/10.5194/acp-8-4605-2008, 2008.

Bond, T., Doherty, S., Fahey, D., Forster, P., Berntsen, T., DeAngelo, B., Flanner, M., Ghan, S., Kärcher, B., Koch, D., Kinne, S., Kondo, Y., Quinn, P., Sarofim, M., Schultz, M., Schulz, M., Venkataraman, C., Zhang, H., Zhang, S., Bellouin, N., Guttikunda, S., Hopke, P., Jacobson, M., Kaiser, J., Klimont, Z., Lohmann, U., Schwarz, J., Shindell, D., Storelvmo, T., Warren, S., and Zender, C.: Bounding the role of black carbon in the climate system: A scientific assessment, J. Geophys. Res., 118, 1–173, https://doi.org/10.1002/jgrd.50171, 2013.

Chakrabarty, R. K., Moosmüller, H., Chen, L.-W. A., Lewis, K., Arnott, W. P., Mazzoleni, C., Dubey, M. K., Wold, C. E., Hao, W. M., and Kreidenweis, S. M.: Brown carbon in tar balls from smoldering biomass combustion, Atmospheric Chemistry and Physics, 10, 6363–6370, https://doi.org/10.5194/acp-10-6363-2010, 2010.

Chakrabarty, R. K., Shetty, N. J., Thind, A. S., Beeler, P., Sumlin, B. J., Zhang, C., Liu, P., Idrobo, J. C., Adachi, K., Wagner, N. L., et al.: Shortwave absorption by wildfire smoke dominated by dark brown carbon, Nature Geoscience, 16, 683–688, 2023.

Cheng, Z., Atwi, K., Onyima, T., and Saleh, R.: Investigating the dependence of light-absorption properties of combustion carbonaceous aerosols on combustion conditions, Aerosol Science and Technology, 53, 419–434, https://doi.org/10.1080/02786826.2019.1566593, 2019.

Claeys, M., Vermeylen, R., Yasmeen, F., Gómez-González, Y., Chi, X., Maenhaut, W., Mészáros, T., and Salma, I.: Chemical characterisation of humic-like substances from urban, rural and tropical biomass burning environments using liquid chromatography with UV/vis photodiode array detection and electrospray ionisation mass spectrometry, Environmental Chemistry, 9, 273–284, 2012.

De Haan, D. O., Corrigan, A. L., Tolbert, M. A., Jimenez, J. L., Wood, S. E., and Turley, J. J.: Secondary organic aerosol formation by self-reactions of methylglyoxal and glyoxal in evaporating droplets, Environmental science & technology, 43, 8184–8190, 2009.

Dinar, E., Taraniuk, I., Graber, E., Anttila, T., Mentel, T. F., and Rudich, Y.: Hygroscopic growth of atmospheric and model humic-like substances, Journal of Geophysical Research: Atmospheres, 112, 2007.

Dinar, E., Riziq, A. A., Spindler, C., Erlick, C., Kiss, G., and Rudich, Y.: The complex refractive index of atmospheric and model humic-like substances (HULIS) retrieved by a cavity ring down aerosol spectrometer (CRD-AS), Faraday discussions, 137, 279–295, 2008.

https://doi.org/10.5194/egusphere-2026-1917
Preprint. Discussion started: 20 May 2026

Dubovik, O. and King, M. D.: A flexible inversion algorithm for retrieval of aerosol optical properties from Sun and sky radiance measurements, Journal of Geophysical Research: Atmospheres, 105, 20 673–20 696, https://doi.org/https://doi.org/10.1029/2000JD900282, 2000.

Fan, X., Song, J., and Peng, P.: Comparison of isolation and quantification methods to measure humic-like substances (HULIS) in atmospheric particles, Atmospheric Environment, 60, 366–374, https://doi.org/https://doi.org/10.1016/j.atmosenv.2012.06.063, 2012.

Graber, E. and Rudich, Y.: Atmospheric HULIS: How humic-like are they? A comprehensive and critical review, Atmospheric Chemistry and Physics, 6, 729–753, 2006.

Guenther, A., Karl, T., Harley, P., Wiedinmyer, C., Palmer, P. I., and Geron, C.: Estimates of global terrestrial isoprene emissions using MEGAN (Model of Emissions of Gases and Aerosols from Nature), Atmospheric Chemistry and Physics, 6, 3181–3210, https://doi.org/10.5194/acp-6-3181-2006, 2006.

Harley, R. A., Hannigan, M. P., and Cass, G. R.: Respeciation of organic gas emissions and the detection of excess unburned gasoline in the atmosphere, Environmental Science & Technology, 26, 2395–2408, 1992.

Hess, M., Koepke, P., and Schult, I.: Optical Properties of Aerosols and Clouds: The Software Package OPAC, Bull. Am. Meteorol. Soc., 79, 831–844, 1998.

Hoffer, A., Gelencsér, A., Guyon, P., Kiss, G., Schmid, O., Frank, G. P., Artaxo, P., and Andreae, M. O.: Optical properties of humic-like substances (HULIS) in biomass-burning aerosols, Atmospheric Chemistry and Physics, 6, 3563–3570, https://doi.org/10.5194/acp-6-3563-2006, 2006.

Hoffer, A., Tóth, A., Nyirő-Kósa, I., Pósfai, M., and Gelencsér, A.: Light absorption properties of laboratory-generated tar ball particles, Atmospheric Chemistry and Physics, 16, 239–246, https://doi.org/10.5194/acp-16-239-2016, 2016.

Hoffmann, T., Odum, J. R., Bowman, F., Collins, D., Klockow, D., Flagan, R. C., and Seinfeld, J. H.: Formation of organic aerosols from the oxidation of biogenic hydrocarbons, Journal of Atmospheric Chemistry, 26, 189–222, 1997.

Hussein, T., Puustinen, A., Aalto, P. P., Mäkelä, J. M., Hämeri, K., and Kulmala, M.: Urban aerosol number size distributions, Atmospheric Chemistry and Physics, 4, 391–411, https://doi.org/10.5194/acp-4-391-2004, 2004.

Kanakidou, M., Seinfeld, J. H., Pandis, S. N., Barnes, I., Dentener, F. J., Facchini, M. C., Van Dingenen, R., Ervens, B., Nenes, A., Nielsen, C. J., Swietlicki, E., Putaud, J. P., Balkanski, Y., Fuzzi, S., Horth, J., Moortgat, G. K., Winterhalter, R., Myhre, C. E. L., Tsigaridis, K., Vignati, E., Stephanou, E. G., and Wilson, J.: Organic aerosol and global climate modelling: a review, Atmospheric Chemistry and Physics, 5, 1053–1123, https://doi.org/10.5194/acp-5-1053-2005, 2005.

Kim, D., Wang, C., Ekman, A. M. L., Barth, M. C., and Rasch, P. J.: Distribution and direct radiative forcing of carbonaceous and sulfate aerosols in an interactive size-resolving aerosol–climate model, Journal of Geophysical Research: Atmospheres, 113, https://doi.org/https://doi.org/10.1029/2007JD009756, 2008.

Kirchstetter, T., Novakov, T., and Hobbs, P.: Evidence that spectral dependence of light absorption by aerosols is affected by organic carbon, J. Geophys. Res., 109, D21208, https://doi.org/10.1029/2004JD004999, 2004.

Kirillova, E. N., Andersson, A., Tiwari, S., Srivastava, A. K., Bisht, D. S., and Gustafsson, O.: Water-soluble organic carbon aerosols during a full New Delhi winter: Isotope-based source apportionment and optical properties, Journal of Geophysical Research: Atmospheres, 119, 3476–3485, https://doi.org/https://doi.org/10.1002/2013JD020041, 2014.

Kleindienst, T. E., Jaoui, M., Lewandowski, M., Offenberg, J. H., Lewis, C. W., Bhave, P. V., and Edney, E. O.: Estimates of the contributions of biogenic and anthropogenic hydrocarbons to secondary organic aerosol at a southeastern US location, Atmospheric environment, 41, 8288–8300, 2007.

https://doi.org/10.5194/egusphere-2026-1917
Preprint. Discussion started: 20 May 2026

Laskin, A., Laskin, J., and Nizkorodov, S. A.: Chemistry of atmospheric brown carbon, Chemical reviews, 115, 4335–4382, 2015.

Li, C., He, Q., Schade, J., Passig, J., Zimmermann, R., Meidan, D., Laskin, A., and Rudich, Y.: Dynamic changes in optical and chemical properties of tar ball aerosols by atmospheric photochemical aging, Atmospheric Chemistry and Physics, 19, 139–163, https://doi.org/10.5194/acp-19-139-2019, 2019.

Li, J., Zhang, Q., Wang, G., Li, J., Wu, C., Liu, L., Wang, J., Jiang, W., Li, L., Ho, K. F., and Cao, J.: Optical properties and molecular compositions of water-soluble and water-insoluble brown carbon (BrC) aerosols in northwest China, Atmospheric Chemistry and Physics, 20, 4889–4904, https://doi.org/10.5194/acp-20-4889-2020, 2020.

Liu, J., Bergin, M., Guo, H., King, L., Kotra, N., Edgerton, E., and Weber, R. J.: Size-resolved measurements of brown carbon in water and methanol extracts and estimates of their contribution to ambient fine-particle light absorption, Atmospheric Chemistry and Physics, 13, 12 389–12 404, https://doi.org/10.5194/acp-13-12389-2013, 2013a.

Liu, P., Zhang, Y., and Martin, S. T.: Complex refractive indices of thin films of secondary organic materials by spectroscopic ellipsometry from 220 to 1200 nm, Environmental science & technology, 47, 13 594–13 601, 2013b.

Liu, P., Abdelmalki, N., Hung, H.-M., Wang, Y., Brune, W., and Martin, S.: Ultraviolet and visible complex refractive indices of secondary organic material produced by photooxidation of the aromatic compounds toluene and m-xylene, Atmospheric Chemistry and Physics, 15, 1435–1446, 2015.

Mathai, S., Veghte, D., Kovarik, L., Mazzoleni, C., Tseng, K.-P., Bucci, S., Capek, T., Cheng, Z., Marinoni, A., and China, S.: Optical Properties of Individual Tar Balls in the Free Troposphere, Environ. Sci. Technol., 57, 16 834–16 842, https://doi.org/10.1021/acs.est.3c03498, 2023.

Mo, Y., Li, J., Liu, J., Zhong, G., Cheng, Z., Tian, C., Chen, Y., and Zhang, G.: The influence of solvent and pH on determination of the light absorption properties of water-soluble brown carbon, Atmospheric Environment, 161, 90–98, https://doi.org/https://doi.org/10.1016/j.atmosenv.2017.04.037, 2017.

Moteki, N., Ohata, S., Yoshida, A., and Adachi, K.: Constraining the complex refractive index of black carbon particles using the complex forward-scattering amplitude, Aerosol Science and Technology, 57, 678–699, 2023.

Nakayama, T., Matsumi, Y., Sato, K., Imamura, T., Yamazaki, A., and Uchiyama, A.: Laboratory studies on optical properties of secondary organic aerosols generated during the photooxidation of toluene and the ozonolysis of α-pinene, Journal of Geophysical Research: Atmospheres, 115, 2010.

Nakayama, T., Sato, K., Matsumi, Y., Imamura, T., Yamazaki, A., and Uchiyama, A.: Wavelength dependence of refractive index of secondary organic aerosols generated during the ozonolysis and photooxidation of α-pinene, Sola, 8, 119–123, 2012.

Nakayama, T., Sato, K., Matsumi, Y., Imamura, T., Yamazaki, A., and Uchiyama, A.: Wavelength and NO x dependent complex refractive index of SOAs generated from the photooxidation of toluene, Atmospheric Chemistry and Physics, 13, 531–545, 2013.

Ng, N. L., Kroll, J. H., Chan, A. W. H., Chhabra, P. S., Flagan, R. C., and Seinfeld, J. H.: Secondary organic aerosol formation from m-xylene, toluene, and benzene, Atmospheric Chemistry and Physics, 7, 3909–3922, https://doi.org/10.5194/acp-7-3909-2007, 2007.

Nguyen, T. B., Lee, P. B., Updyke, K. M., Bones, D. L., Laskin, J., Laskin, A., and Nizkorodov, S. A.: Formation of nitrogen-and sulfur-containing light-absorbing compounds accelerated by evaporation of water from secondary organic aerosols, Journal of Geophysical Research: Atmospheres, 117, 2012.

Odum, J. R., Hoffmann, T., Bowman, F., Collins, D., Flagan, R. C., and Seinfeld, J. H.: Gas/Particle Partitioning and Secondary Organic Aerosol Yields, Environmental Science & Technology, 30, 2580–2585, https://doi.org/10.1021/es950943+, 1996.

https://doi.org/10.5194/egusphere-2026-1917
Preprint. Discussion started: 20 May 2026

Olivier, J., Bouwman, A., Van der Maas, C., Berdowslci, J., Veldt, C., Bloos, J., Visschedijk, A., Zandyelt, P., and Haverlag, J.: De-scription of EDGAR Version 2.0, A set of global emission inventories of greenhouse gases and ozone-depleting sub-stances for all anthropogenic and most natural sources on a per country basis and on, 1, 1996.

Powelson, M. H., Espelien, B. M., Hawkins, L. N., Galloway, M. M., and De Haan, D. O.: Brown carbon formation by aqueous-phase carbonyl compound reactions with amines and ammonium sulfate, Environmental science & technology, 48, 985–993, 2014.

Ramanathan, V., Li, F., Ramana, M., Praveen, P., Kim, D., Corrigan, C., Nguyen, H., Stone, E. A., Schauer, J. J., Carmichael, G., et al.: Atmospheric brown clouds: Hemispherical and regional variations in long-range transport, absorption, and radiative forcing, Journal of Geophysical Research: Atmospheres, 112, 2007.

Rissler, J., Vestin, A., Swietlicki, E., Fisch, G., Zhou, J., Artaxo, P., and Andreae, M. O.: Size distribution and hygroscopic prop-erties of aerosol particles from dry-season biomass burning in Amazonia, Atmospheric Chemistry and Physics, 6, 471–491, https://doi.org/10.5194/acp-6-471-2006, 2006.

Romonosky, D. E., Ali, N. N., Saiduddin, M. N., Wu, M., Lee, H. J. J., Aiona, P. K., and Nizkorodov, S. A.: Effective absorption cross sections and photolysis rates of anthropogenic and biogenic secondary organic aerosols, Atmospheric Environment, 130, 172–179, https://doi.org/https://doi.org/10.1016/j.atmosenv.2015.10.019, chemical Characterization of Secondary Organic Aerosol - Dedication to Professor Claeys, 2016.

Saleh, R.: From measurements to models: toward accurate representation of brown carbon in climate calculations, Current Pollution Reports, 6, 90–104, 2020.

Saleh, R., Robinson, E., Tkacik, D., Ahern, A., Liu, S., Aiken, A., Sullivan, R., Presto, A., Dubey, M., Yokelson, R., Donahue, N., and Robinson, A.: Brownness of organics in aerosols from biomass burning linked to their black carbon content, Nature Geoscience, 7, 647–650, https://doi.org/10.1038/NGEO2220, 2014.

Sand, M., Samset, B., Myhre, G., Gliß, J., Bauer, S., Bian, H., Chin, M., Checa-Garcia, R., Ginoux, P., Kipling, Z., Kirkevåg, A., Kokkola, H., Sager, P. L., Lund, M., Matsui, H., van Noije, T., Olivié, D., Rémy, S., Schulz, M., Stier, P., Stjern, C., Takemura, T., Tsigaridis, K., Tsyro, S., and Watson-Parris, D.: Aerosol absorption in global models from AeroCom phase III, Atmos. Chem. Phys., 21, 15 929–15 947, https://doi.org/10.5194/acp-21-15929-2021, 2021.

Sedlacek III, A. J., Buseck, P. R., Adachi, K., Onasch, T. B., Springston, S. R., and Kleinman, L.: Formation and evolution of tar balls from northwestern US wildfires, Atmospheric Chemistry and Physics, 18, 11 289–11 301, https://doi.org/10.5194/acp-18-11289-2018, 2018.

Sindelarova, K., Granier, C., Bouarar, I., Guenther, A., Tilmes, S., Stavrakou, T., Müller, J.-F., Kuhn, U., Stefani, P., and Knorr, W.: Global data set of biogenic VOC emissions calculated by the MEGAN model over the last 30 years, Atmospheric Chemistry and Physics, 14, 9317–9341, https://doi.org/10.5194/acp-14-9317-2014, 2014.

Sumlin, B. J., Pandey, A., Walker, M. J., Pattison, R. S., Williams, B. J., and Chakrabarty, R. K.: Atmospheric photooxidation diminishes light absorption by primary brown carbon aerosol from biomass burning, Environmental Science & Technology Letters, 4, 540–545, 2017.

Sumlin, B. J., Heinson, W. R., and Chakrabarty, R. K.: Retrieving the aerosol complex refractive index using PyMieScatt: A Mie compu-tational package with visualization capabilities, J. Quant. Spect. Rad. Trans., 205, 127–134, https://doi.org/10.1016/j.jqsrt.2017.10.012, 2018.

Updyke, K. M., Nguyen, T. B., and Nizkorodov, S. A.: Formation of brown carbon via reactions of ammonia with secondary organic aerosols from biogenic and anthropogenic precursors, Atmospheric environment, 63, 22–31, 2012.

Wang, H., Liu, X., Wu, C., and Lin, G.: Regional to global distributions, trends, and drivers of biogenic volatile organic compound emission from 2001 to 2020, Atmospheric Chemistry and Physics, 24, 3309–3328, https://doi.org/10.5194/acp-24-3309-2024, 2024.

https://doi.org/10.5194/egusphere-2026-1917
Preprint. Discussion started: 20 May 2026

Washenfelder, R., Flores, J., Brock, C., Brown, S., and Rudich, Y.: Broadband measurements of aerosol extinction in the ultraviolet spectral region, Atmospheric Measurement Techniques, 6, 861–877, 2013.

Wiscombe, W. J.: Improved Mie scattering algorithms, Appl. Opt., 19, 1505–1509, https://doi.org/10.1364/AO.19.001505, 1980.

Wu, G., Ram, K., Fu, P., Wang, W., Zhang, Y., Liu, X., Stone, E. A., Pradhan, B. B., Dangol, P. M., Panday, A. K., Wan, X., Bai, Z., Kang, S., Zhang, Q., and Cong, Z.: Water-Soluble Brown Carbon in Atmospheric Aerosols from Godavari (Nepal), a Regional Representative of South Asia, Environmental Science & Technology, 53, 3471–3479, https://doi.org/10.1021/acs.est.9b00596, pMID: 30848122, 2019.

Zhong, M. and Jang, M.: Light absorption coefficient measurement of SOA using a UV–Visible spectrometer connected with an integrating sphere, Atmospheric environment, 45, 4263–4271, 2011.